Dalton Transactions

PAPER

Formation of cyanates in low-valent uranium chemistry: a synergistic experimental/theoretical study†

Cite this: *Dalton Trans.*, 2014, **43**, 11202

Christos E. Kefalidis,[a] Alistair S. P. Frey,[b] S. Mark Roe,[b] F. Geoffrey N. Cloke*[b] and Laurent Maron*[a]

Received 28th February 2014,
Accepted 3rd April 2014

DOI: 10.1039/c4dt00618f

www.rsc.org/dalton

Computational studies on the reductive activation of a mixture of CO and NO by the U(III) complex [U(η-C_8H_6{Si^iPr_3-1,4}$_2$)(η-Cp*)], which affords a mixture of [U(η-C_8H_6{Si^iPr_3-1,4}$_2$)(η-Cp*)]$_2$(μ-OCN)$_2$ **1** and [U(η-C_8H_6{Si^iPr_3-1,4}$_2$)(η-Cp*)]$_2$(μ-O) **2**, show that the reaction proceeds *via* an initial attack of CO on a μ–η^2:η^2 coordinated NO, side-on bridged between two uranium centres. This leads to the formation of the bridging oxo complex **2** and the cyanate radical; coordination of the latter to the starting complex and dimerisation affords **1**. The DFT studies also predict the existence of the monocyanate-bridged, mixed valence species [U(η-C_8H_6{Si^iPr_3-1,4}$_2$)(η-Cp*)]$_2$(μ-OCN) **3**, which has now been experimentally observed.

Introduction

Low-valent uranium complexes, especially those of U(III), have attracted much attention in recent years in the field of small molecule activation requiring highly reducing metal complexes. Reductive chemistry of N_2, CO, and CO_2 has all featured prominently in this area, which has recently been comprehensively reviewed.[1] DFT computational studies have proved crucial in understanding and rationalising the reactivity and structure, for example in the reduction of N_2,[2] reductive cyclisation of CO,[3] and reductive disproportionation of CO_2.[4] We have recently described the reductive activation of a mixture of CO and NO by the mixed sandwich U(III) complex [U(η-C_8H_6{Si^iPr_3-1,4}$_2$)(η-Cp*)], which affords a mixture of the bridging oxo complex [U(η-C_8H_6{Si^iPr_3-1,4}$_2$)(η-Cp*)]$_2$(μ-O) and the doubly cyanate bridged complex [U(η-C_8H_6{Si^iPr_3-1,4}$_2$)(η-Cp*)]$_2$(μ-OCN)$_2$.[5] Herein we report a joint experimental/theoretical study on defining the reaction mechanism of this novel transformation. The synergy between theory and experiment allows one to demonstrate that the mechanism involves a bimetallic species with an unusual μ–η^2:η^2 coordination of NO, similar to that reported in the case of CO by Mckay *et al.*[3] In addition, DFT calculations suggested the potential existence of a monocyanate-bridged mixed valence species, which has now been experimentally verified.

Computational details

All the structures reported in this study were fully optimized with the Becke's 3-parameter hybrid functional[6] combined with the non-local correlation functional provided by Perdew/Wang[7] (denoted as B3PW91). For the estimation of the redox step of the NO reduction by the uranium(III) system a Hess–Born–Haber cycle method is used, as proposed by Castro *et al.*[4a] For this step, the relativistic energy-consistent small-core pseudopotential obtained from the Stuttgart-Köln ECP library has been used in combination with its adapted segmented basis set.[8] For the reaction steps involving intermediates in which the uranium's oxidation state is fixed to +IV, the corresponding 5f-in-large-core ECP (augmented by a f polarization function, α = 1.0) was used.[9] The aforementioned computational scheme was found previously by our group to give coherent results.[4b,10] For the silicon atoms the quasi-relativistic energy-adjusted *ab initio* pseudopotential was used, along with its corresponding energy-optimized valence basis set,[11] augmented by a d polarization function.[12] For the remaining atoms the 6-31G(d,p) basis set was used.[13,14] In all computations no constraints were imposed on the geometry. All stationary points have been identified as minima (number of imaginary frequencies N_{imag} = 0) or transition states (N_{imag} = 1). Intrinsic reaction paths (IRPs)[15] were traced from the various transition structures to make sure that no further

[a]*Université de Toulouse et CNRS, INSA, UPS, UMR 5215, LPCNO, 135 Avenue de Rangueil, F-31077 Toulouse, France. E-mail: laurent.maron@irsamc.ups-tlse.fr*
[b]*Department of Chemistry, School of Life Sciences, University of Sussex, Brighton, BN1 9QJ, UK*

†Electronic supplementary information (ESI) available. See DOI: 10.1039/c4dt00618f

intermediates exist. The vibrational modes and the corresponding frequencies are based on a harmonic force field. Enthalpy energies were obtained at T = 298.15 K within the harmonic approximation. The ^{i}Pr substituents of the silicon atoms of the side arms of the experimentally used COT ligand have been replaced by hydrogens. This simplification is not changing the results as it has been shown in a previous study in a related ligand environment.[3] The GAUSSIAN09 program suite was used in all calculations.[16] Finally, for the 3D representation of the structures the Cylview[17] graphical program was used, and Chemcraft[18] was used for the visualization of the molecular orbitals.

Experimental section

General methods

Unless specified otherwise all manipulations were carried out using conventional high vacuum and Schlenk line techniques, under an atmosphere of dry argon, or under a dinitrogen atmosphere in an MBraun glove box. Solvents were refluxed over suitable drying agents under a dinitrogen atmosphere, and distilled and degassed prior to use: toluene was refluxed over sodium; THF was refluxed over potassium; pentane was refluxed over sodium/potassium alloy. d_8-Toluene was dried by refluxing over sodium and then vacuum transferred into an ampoule and stored under dinitrogen prior to use. ^{1}H and ^{13}C NMR spectra were recorded on a Varian VNMRS 400 spectrometer at room temperature, unless otherwise stated. Chemical shifts reported in ppm (δ) are relative to the residual proton chemical shift of the deuterated solvent (^{1}H) or the carbon chemical shift of the deuterated solvent (^{13}C). Mass spectra were recorded on a VG autospec Fisons instrument (electron impact ionisation at 70 eV). Gas transfer was *via* a Toepler pump with calibrated (by transfer of xenon into a receiving vessel of accurately known volume, and differential weighing) delivery pressure. Control of the stoichiometry of the gas reactions was achieved by the use of standard 5 mm (for the NMR studies) or shortened 10 mm (for preparative scale) Young's NMR tubes of accurately known volume containing measured volumes (microlitre syringe) of solvent (and therefore of known headspace). [U(η-C$_8$H$_6${Si^{i}Pr$_3$-1,4}$_2$)(η-Cp*)THF] was prepared as previously described.[19] High purity NO was prepared by treatment of nitrosyl sulphuric acid with mercury,[20] and purified by transferring through a column of KOH pellets into a 1 litre storage bulb on the Toepler pump line. ^{13}CO (99% enriched, Cambridge Isotopes) was used as supplied.

Synthesis of [U(η-C$_8$H$_6${Si^{i}Pr$_3$-1,4}$_2$)(η-Cp*)]$_2$(μ-OCN) 3. A sample of black, crystalline [U(η-C$_8$H$_6${Si^{i}Pr$_3$-1,4}$_2$)(η-Cp*)]-(THF) (400 mg, 4.64 × 10^{-4} mol) was placed in an ampoule (high-vacuum PTFE stopcock, 50 mL volume) and heated under vacuum (110 °C/1 × 10^{-5} mbar) for 1 h. The desolvated material was dissolved in d_8-toluene (0.5 mL). The solution was cooled to −78 °C, the headspace evacuated and ^{13}CO (0.07 bar, 1.55 × 10^{-4} mol) was admitted followed by NO (0.07 bar, 1.55 × 10^{-4} mol). The flask was warmed to ambient temperature resulting in a change in colour to red-brown. Standing at ambient temperature for 5 days, −50 °C for 3 days and 4 °C for 3 days gave the product as black crystals. The product was rinsed with pentane at 0 °C (significant amount of product was lost to dissolution during rinsing) and dried *in vacuo* to afford the title compound as black prisms suitable for single crystal X-ray diffraction (10 mg, 3% based on starting [U(*h*-C$_8$H$_6${Si^{i}Pr$_3$-1,4}$_2$)(*h*-Cp*)](THF)).

^{1}H NMR (C$_6$D$_5$CD$_3$, 303 K): δ ppm 67.1 (s, 2H, COT ring-C*H*), 34.6 (s, 2H, COT ring-C*H*), 6.43 (s, 15H, Cp*–C*H*$_3$), −1.33 (6H, s, ^{i}Pr–C*H*), −3.82 (18H, s, ^{i}Pr–C*H*$_3$), −7.01 (18H, s, ^{i}Pr–C*H*$_3$), −8.29 (18H, s, br, ^{i}Pr–C*H*$_3$), −8.63 (24H, s, br, ^{i}Pr–C*H*$_3$ and ^{i}Pr–C*H*), −14.6 (s, br, 15H, Cp*–C*H*$_3$), −73.7 (s, 2H, COT ring-C*H*), −83.0 (s, 2H, COT ring-C*H*), −99.4 (s, 2H, COT ring-C*H*), −114 (s, 2H, COT ring-C*H*). ^{13}C NMR (C$_6$D$_5$CD$_3$, 303 K, selected data): δ ppm 223.5. MS (EI): m/z = 832 (65%, [(η-C$_8$H$_6${Si^{i}Pr$_3$-1,4}$_2$)(η-Cp*)U(O^{13}CN)]$^{+}$).The crystal structure of **3** has been deposited at the Cambridge Crystallographic Data Centre and allocated the deposition number 988885. For details of data collection and refinement see ESI.†

Results and discussion

The previously reported, overall experimental result is shown in Scheme 1.[5]

The initial coordination of the highly reactive nitric oxide (in preference to carbon monoxide) substrate to the uranium(III) complex precursor can be achieved in two different ways: in a terminal fashion, through nitrogen atoms or in a side-on fashion, involving the π_{NO}. This is the first plausible step in the reaction sequence which, upon an electrophilic attack of the CO, ultimately yields the doubly bridged cyanate bis-uranium complex **1** along with the bridging oxo-species **2** (Scheme 1). Due to the presence of unpaired electrons in the uranium(III) fragment as well as in the NO substrate, all possible spin state combinations with the two different bonding modes of the NO in the initially formed adducts have to be

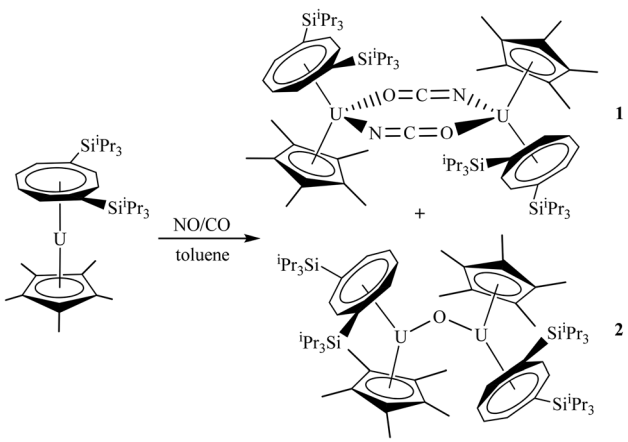

Scheme 1 Reaction of [U(η-C$_8$H$_6${Si^{i}Pr$_3$-1,4}$_2$)(η-Cp*)] with NO and CO in toluene.

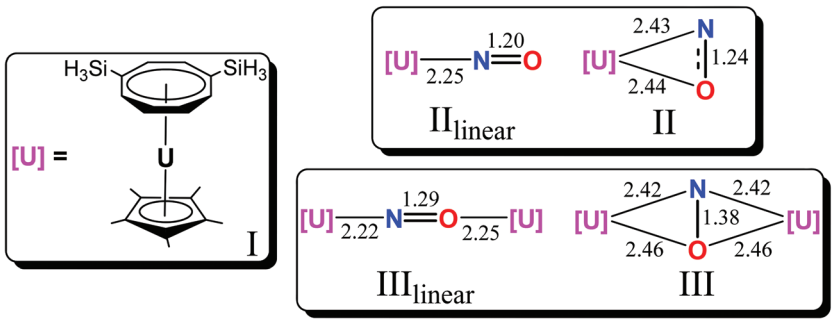

Scheme 2 Structures of different coordination modes of NO on mono- and bimetallic uranium(IV) complexes. All the given distances are in angstroms (Å).

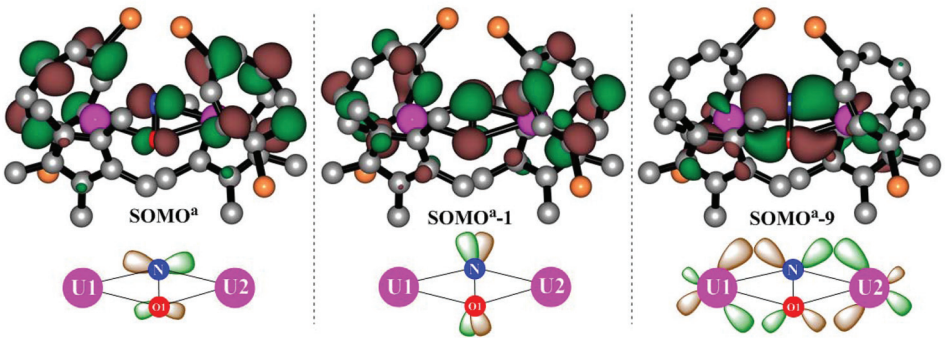

Fig. 1 Selected frontier occupied molecular orbitals for intermediate **III**.

considered. The results are depicted in Scheme S1.† The most stable adduct is found to be terminally bonded NO in its quintet spin state (4 unpaired electrons), which implies a partial oxidation of the uranium centre. In particular, its electronic configuration (EC) is $5f^{2.6}\ \pi^{*1.5}_{NO}$, based on the Mulliken atomic spin densities. The next most stable complex (1.3 kcal mol^{-1} higher in energy) has the same type of bonding mode for the NO substrate but in its triplet state (2 unpaired electrons). For the latter, based on its Mulliken atomic spin densities, the uranium has an EC of $5f^{2.2}$ with the NO fragment forming a pair of electrons and developing a consequently stronger bond with the uranium atom. The latter is also reflected in a decrease of the U–N bond distance with respect to that in the quintet state (by 0.17 Å). Finally, the singlet spin state (0 unpaired electrons) of the terminally bound NO complex is 10.5 kcal mol^{-1} higher in energy than the most stable (quintet) spin state, making its existence unlikely. The singlet spin state describes an electronic situation where there are no unpaired electrons on either the uranium atom or the nitric oxide ligand. Identical electronic configurations have been found for the respective η^2-bound complexes, although they are slightly higher in energy than the most stable linear complex by 3.7, 2.8, and 5.5 kcal mol^{-1} for the singlet, triplet, and quintet spin states, respectively. As these energy differences are within the precision of the method,[21] the NO coordination can easily induce oxidation of the uranium centre upon η^2 coordination as well. Indeed, using the 5f-in-core RECPs fixed in the oxidation state IV for the uranium, the side-on coordination is found to be more stable by 5.1 kcal mol^{-1} compared to the terminal nitrosyl analogue. It should be noted that in the η^2-bound NO, the N–O bond length of 1.24 Å is 0.04 Å greater than that in the terminal NO complex, and is hence more reminiscent of a mono-reduced substrate (d_{NO} = 1.27 Å for the free $(NO^{\bullet})^-$ molecule, see ESI†). This behaviour is probably due to the better overlap of the d orbital of the uranium centre with that of the π bond of the NO. This transient species readily coordinates a second uranium(III) fragment in a μ–η^2:η^2 fashion (**III** in Scheme 2), thus inducing a second single electron transfer to the already mono-reduced nitrosyl substrate. This coordination results in an extra energetic stabilization, in line with the stability of related bimetallic species already reported in the literature for other substrates.[3,4,10c] Overall, the exothermicity of the double reduction of the NO by the two uranium centers is found to be −60.5 kcal mol^{-1}.

Close inspection of some important molecular orbitals of the "key intermediate" **III** clearly reveals the bonding situation. In particular, $SOMO^a$ and $SOMO^a$−1 correspond to the antibonding lone pairs of the bridged NO (Fig. 1). These two molecular orbitals are perpendicular to each other and their nodal planes do not share the same plane with the two uranium atoms, being slightly rotated. This is consistent with the dianionic character of the NO bridged moiety, which accumulates most of the negative charge resulting from the two consecutive one electron oxidations of each uranium centre. This makes

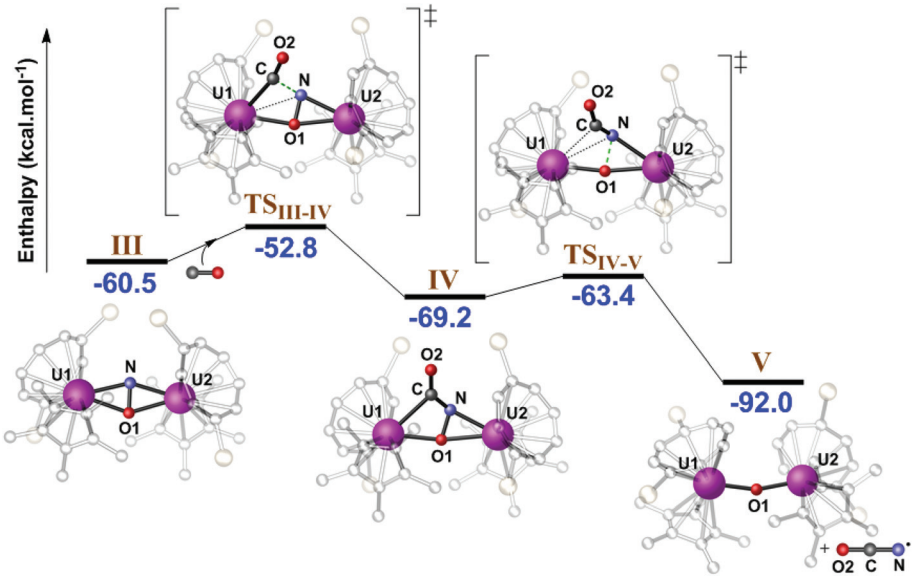

Fig. 2 Energy reaction profile for the electrophilic attack of CO molecule on intermediate III leading to complex V.

complex **III** highly nucleophilic, and able to react with substrates like CO. The molecular orbital (SOMO[a]−9) in intermediate **III** explains the bonding situation between the uranium centres and the μ–η^2:η^2 bridging mode of the NO (Fig. 1). In particular, the latter involves d orbitals of the two uranium atoms interacting with a vacant π* orbital of the NO.

Mechanism

As the coordination of the NO in intermediate **III** is a highly exothermic process (−60.5 kcal mol^{-1} with respect to the reactants, *vide supra*), the reaction profile will be described from complex **III** (Fig. 2). It should be noted that other possible mechanistic scenarios have been considered computationally: for example, the cleavage of the NO bond instead of the electrophilic attack by CO, which has been excluded since it resulted in the formation of a highly unstable mixed valence U(v)/U(vi) species.

The reaction can proceed then through the $\mathbf{TS_{III–IV}}$, namely an electrophilic attack of CO on the doubly reduced NO. In $\mathbf{TS_{III–IV}}$, the distance between the carbon of the CO group and the nitrogen of NO remains long (2.05 Å) allowing an extra interaction between the carbon of CO and the U1 centre ($d_{U1–C}$ = 2.58 Å). The N–O1 bond distance remains almost unchanged with respect to the intermediate **III** (1.37 and 1.38 Å respectively). On the other hand, the bonding distance between the U1 and the ancillary ligands (Cp* and COT) is increased significantly with respect to **III**, by 0.5 Å. The latter is essential for the electrophilic attack to occur. The electrophilic nature of this reaction can be seen by inspection of the molecular orbitals of the transition state $\mathbf{TS_{III–IV}}$ (see Fig. 3): the SOMO[a] orbital of $\mathbf{TS_{III–IV}}$ results from the overlap between the SOMO[a] of **III**, which corresponds to the lone pair of the NO, with the LUMO of the CO. It is also interesting to note that the LUMO of the $\mathbf{TS_{III–IV}}$ is a combination of a non-bonding available d orbital of the U1 atom with the second degenerate π* orbital of CO, which probably accounts for the low-energy transition state (Fig. 3).

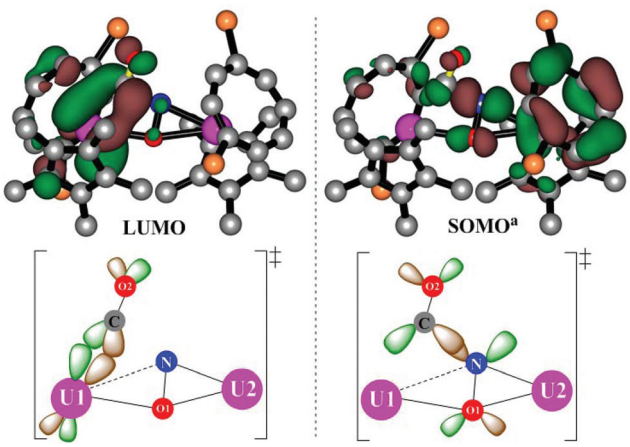

Fig. 3 Frontier molecular orbitals of $\mathbf{TS_{III–IV}}$.

In terms of kinetics, this step involves an activation barrier of only 7.7 kcal mol^{-1}, and thermodynamically corresponds to a process which is exothermic by 8.8 kcal mol^{-1}. In the resulting intermediate **IV**, the O1–N–C–O2 moiety displays a zig-zag configuration with the C and O1 having a κ^2 coordination mode with the U1 centre, whereas the U2 atom is ligated in a η^2-fashion to the N–O1 bond. The N–O1 bond in **IV** is elongated by 0.08 Å compared to that in the intermediate **III**, and is further activated by passing through $\mathbf{TS_{IV–V}}$, requiring again a small activation barrier (5.8 kcal mol^{-1}). At the transition state, $\mathbf{TS_{IV–V}}$, the interatomic distance between N and O1 is 1.69 Å, corresponding to an increase of 0.24 Å compared to the corresponding intermediate **IV**. The product of this step is

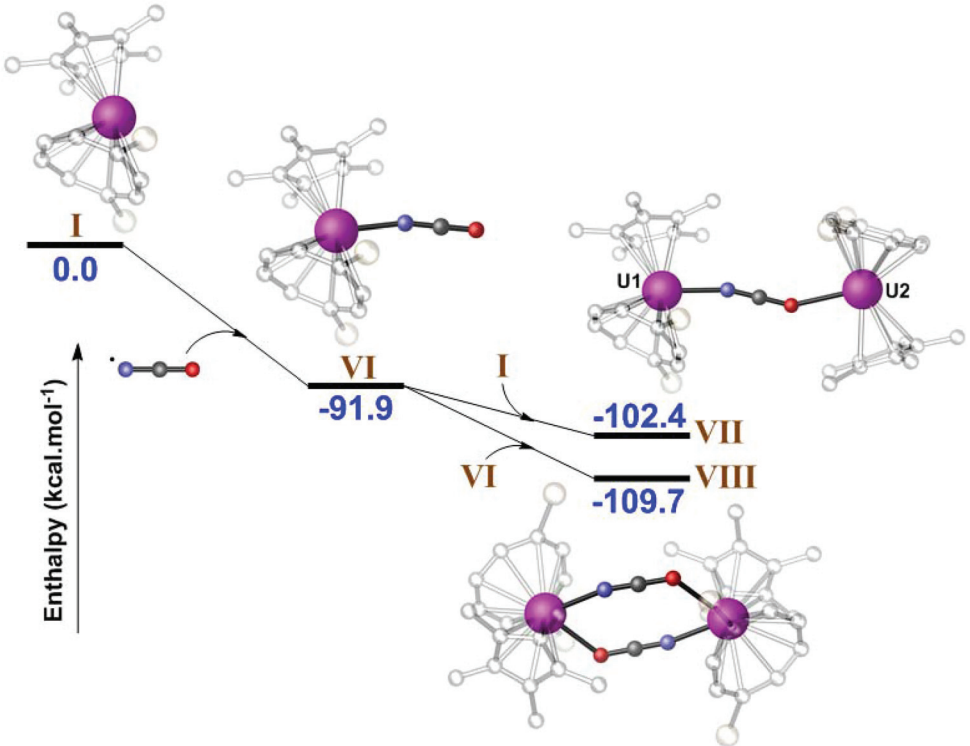

Fig. 4 Pathways for the trapping of the NCO radical by precursor complex **I**.

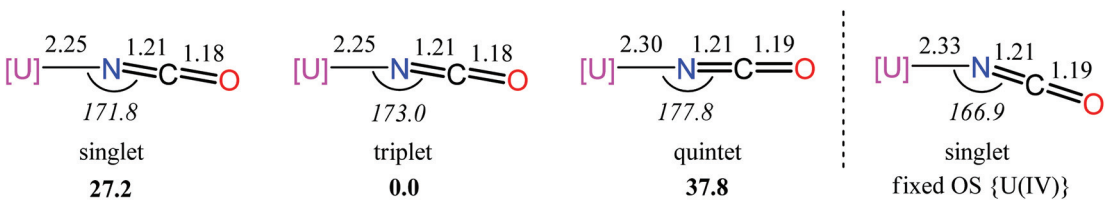

Scheme 3 Possible spin states for the monomeric structure of binding cyanates.

the oxo-intermediate **V**. It is noteworthy that the calculated geometry is in good agreement with the experimentally derived structure, with $d_{average}$(U–O) = 2.17 Å, compared to the experimental value of 2.11 Å. The bond angle U1–O1–U2 is found to be 161.5, 7° smaller than the experimental value, a difference which is mainly due to the absence of the steric effects induced by the ^{i}Pr groups which are absent in our simplified system. Finally, this step is found to be exothermic by 22.8 kcal mol^{-1}, even though the concomitant release of the CNO radical occurs. The latter highly reactive radical can then bind to the precursor complex **I** to form a very stable complex **VI**, in which the NCO$^{\bullet}$ is bound through its nitrogen atom (Fig. 4), and which results in a large stabilization of 91.9 kcal mol^{-1}.

The electronic configuration of this highly stable cyanate intermediate **VI** requires some analysis. To that effect, different spin states for this intermediate (singlet, triplet and quintet) were computed. Ideally, in the closed-shell singlet spin state, two electrons of the uranium atom form a lone pair, while the third one forms a bonding electron pair with the cyanate radical. The triplet state corresponds to an electron configuration where the uranium atom possesses two unpaired electrons and a bonding pair with the NCO group. Finally, the quintet spin state corresponds to a loosely bonded cyanate adduct, having all the electrons unpaired (three on uranium and one on NCO). It is worth noting that the two former spin states correspond to a uranium(IV) system whereas the latter corresponds to a U(III) complex. The calculations predict that the spin triplet state is the most stable compared to the other two, by more than 27 kcal mol^{-1}. The U–N bond lengths in the singlet and the triplet spin states are shorter by only 0.05 Å compared to the quintet, while all the other significant bond lengths, such as N=C and C=O, are essentially the same as in the free NCO radical (Scheme 3 and Scheme S1†). In the triplet spin state, the spin density of the uranium is 2.36|e|. Some residual negative charge is located at the carbon atoms of the COT ligand and at the nitrogen atom of the NCO fragment. Examination of the Mulliken spin densities of the quintet spin

state reveals that the uranium atom has a spin density of 3.17, 0.17|e| higher than the ideal, without any sizeable spin density at the NCO ligand. This extra density is found to be accumulated on some carbon atoms of the COT ligand, resulting in distortion of the COT ligand, and the consequent estimated energy increase. The latter is due to the inability of the NCO fragment to receive more density from the metal.

Despite its high energetic stability, intermediate **VI** can anchor another uranium(III) species to form the bimetallic complex **VII** (Fig. 4). The formation of the latter species is an exothermic process (10.5 kcal mol^{-1} more stable than intermediate **VI**). This intermediate is interesting as it corresponds to a mix-valence complex with U(IV) and U(III) metal centres. In terms of geometrical features, the U1–N and C═O bond distances are slightly elongated by 0.07 and 0.01 Å respectively, while the N═C bond decreased by only 0.02 Å with respect to intermediate **VI**. These small differences are the result of the newly formed bond between the second uranium centre and the oxygen centre (2.67 Å). Moreover, the bond angle U1–N–C decreases by almost 5 degrees, with respect to the intermediate **VI**, while the bond angle U2–O–C decreases to 153.0°. Alternatively, intermediate **VI** may dimerise to form complex **VIII**, *i.e.* the experimentally observed product **1** in Scheme 1, as previously reported.[5] This process is predicted to be exothermic by 17.8 kcal mol^{-1}, being however only 7.3 kcal mol^{-1} more stable than the mixed valence complex **VII**. Thus, one can conclude that both complexes **VII** and **VIII** may exist. Indeed, by a slight change in the stoichiometry of the reaction (see Experimental section), we have now found that the mixed valence compound **VII** (**3** in Scheme 4 below) maybe isolated in small amounts together with the bridging oxo compound **2**. Complex **3** displays an ^{1}H NMR spectrum in which the ligand resonances associated with the two uranium centres are clearly different, consistent with the non-centrosymmetric structure imposed by the single cyanate bridge. A resonance at δ ppm 223.5 in the $^{13}C\{^{1}H\}$ NMR spectrum of **3** is assigned to the single bridging cyanate carbon, and maybe compared to that at δ ppm 249.3 for the doubly bridging cyanate ligands in **1**.

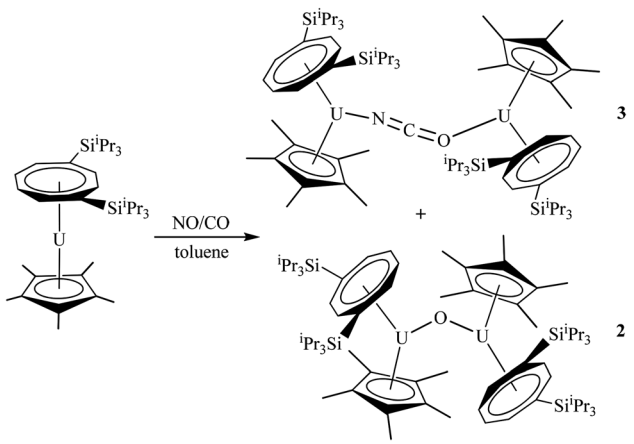

Scheme 4 Reaction of [U(η-C_8H_6{Si^iPr_3-1,4}$_2$)(η-Cp*)] with NO and CO in toluene, using a modified stoichiometry.

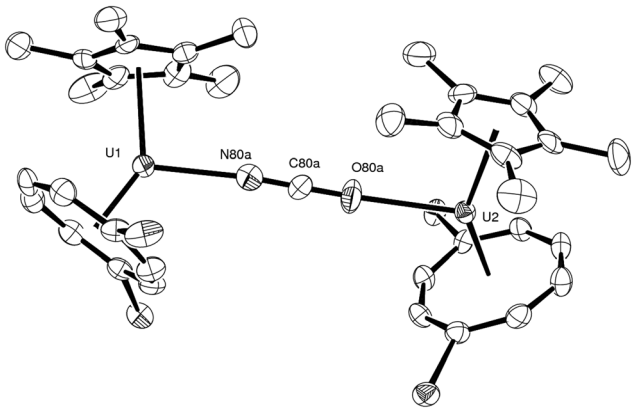

Fig. 5 The X-ray structure of **3** (thermal ellipsoids at 30%, hydrogens and isopropyl groups are removed for clarity).

The structure of **3**, as determined by X-ray crystallography, is shown in Fig. 5. The structure includes a single bridging cyanate moiety, but the cyanate is disordered, both linearly, *i.e.* N–C–O over O–C–N, and radially. This required that the cyanate moiety be heavily restrained to expected values and, as such, no meaningful inferences can be made about the bond lengths and angles in and around the bridging cyanate group. Several models can be constructed that refine equally well, but crucially there is no evidence for a second bridging cyanate. Similar disorder issues were encountered in the X-ray structure of the doubly bridged cyanate complex **1**.[5]

Conclusions

DFT computational studies on the reductive activation of a mixture of CO and NO by the U(III) complex [U(η-C_8H_6{Si^iPr_3-1,4}$_2$)(η-Cp*)], which affords a mixture of [U(η-C_8H_6{Si^iPr_3-1,4}$_2$)(η-Cp*)]$_2$(μ-OCN)$_2$ **1** and [U(η-C_8H_6{Si^iPr_3-1,4}$_2$)(η-Cp*)]$_2$(μ-O) **2**, show that the reaction proceeds *via* an initial attack of CO on a dimeric intermediate containing an μ–η^2:η^2 coordinated NO. This leads to the formation of the bridging oxo complex **2** and the cyanate radical, which is trapped by the starting complex [U(η-C_8H_6{Si^iPr_3-1,4}$_2$)(η-Cp*)] to afford [U(η-C_8H_6{Si^iPr_3-1,4}$_2$)(η-Cp*)(NCO)]. Theory suggests that the latter can either dimerise to afford the previously experimentally observed, doubly cyanate-bridged dimer [U(η-C_8H_6{Si^iPr_3-1,4}$_2$)(η-Cp*)]$_2$(μ-OCN)$_2$ **1** or coordinate a second molecule of the starting complex [U(η-C_8H_6{Si^iPr_3-1,4}$_2$)(η-Cp*)] to yield the mixed valence species [U(η-C_8H_6{Si^iPr_3-1,4}$_2$)(η-Cp*)]$_2$(μ-OCN). This mixed valence species **3** has now been isolated from the reaction mixture for the first time and crystallographically characterised, thus confirming the outcome predicted by the computational studies.

Acknowledgements

We thank the European Research Council for support. CINES and CalMip are acknowledged for a generous grant of computing time. LM is also grateful to the Humboldt Foundation.

References

1 (*a*) P. Arnold, *Chem. Commun.*, 2011, **47**, 9005–9010; (*b*) B. M. Gardner and S. T. Liddle, *Eur. J. Inorg. Chem.*, 2013, 3753–3770; (*c*) O. P. Lam and K. Meyer, *Polyhedron*, 2012, **32**, 1–96; (*d*) H. S. La Pierre and K. Meyer, *Prog. Inorg. Chem.*, 2014, **58**, in press.

2 F. G. N. Cloke, J. C. Green and N. Kaltsoyannis, *Organometallics*, 2004, **23**, 832–835.

3 D. McKay, A. Frey, J. C. Green, F. G. N. Cloke and L. Maron, *Chem. Commun.*, 2012, **48**, 4118–4120.

4 (*a*) L. Castro, O. P. Lam, S. C. Bart, K. Meyer and L. Maron, *Organometallics*, 2010, **29**, 5504–5510; (*b*) V. Mougel, C. Camp, J. Pécaut, C. Copéret, L. Maron, C. E. Kefalidis and M. Mazzanti, *Angew. Chem., Int. Ed.*, 2012, **51**, 12280–12284.

5 A. S. P. Frey, F. G. N. Cloke, M. P. Coles and P. B. Hitchcock, *Chem. – Eur. J.*, 2010, **16**, 9446–9448.

6 A. D. Becke, *J. Chem. Phys.*, 1993, **98**, 5648–5652.

7 J. P. Perdew and Y. Wang, *Phys. Rev. B: Condens. Matter*, 1992, **45**, 13244–13249.

8 (*a*) W. Küchle, M. Dolg, H. Stoll and H. Preuß, *J. Chem. Phys.*, 1994, **100**, 7535–7543; (*b*) X. Y. Cao, M. Dolg and H. Stoll, *J. Chem. Phys.*, 2003, **118**, 487–497; (*c*) X. Cao and M. Dolg, *J. Mol. Struct. (THEOCHEM)*, 2004, **673**, 203–209.

9 A. Moritz, X. Y. Cao and M. Dolg, *Theor. Chem. Acc.*, 2007, **118**, 845–854.

10 (*a*) L. Castro, A. Yahia and L. Maron, *ChemPhysChem*, 2010, **11**, 990–994; (*b*) L. Castro, A. Yahia and L. Maron, *Dalton Trans.*, 2010, **39**, 6682–6692; (*c*) B. Kosog, C. E. Kefalidis, F. W. Heinemann, L. Maron and K. Meyer, *J. Am. Chem. Soc.*, 2012, **134**, 12792–12797.

11 A. Bergner, M. Dolg, W. Küchle, H. Stoll and H. Preuß, *Mol. Phys.*, 1993, **80**, 1431–1441.

12 A. W. Ehlers, M. Böhme, S. Dapprich, A. Gobbi, A. Höllwarth, V. Jonas, K. F. Köhler, R. Stegmann, A. Veldkamp and G. Frenking, *Chem. Phys. Lett.*, 1993, **208**, 111–114.

13 (*a*) W. J. Hehre, R. Ditchfield and J. A. Pople, *J. Chem. Phys.*, 1972, **56**, 2257–2261; (*b*) P. C. Hariharan and J. A. Pople, *Theor. Chim. Acta*, 1973, **28**, 213–222.

14 J. S. Binkley, J. A. Pople and W. J. Hehre, *J. Am. Chem. Soc.*, 1980, **102**, 939–947.

15 (*a*) C. Gonzalez and H. B. Schlegel, *J. Chem. Phys.*, 1989, **90**, 2154–2161; (*b*) C. Gonzalez and H. B. Schlegel, *J. Phys. Chem.*, 1990, **94**, 5523–5527.

16 M. J. Frisch, G. W. Trucks, H. B. Schlegel, G. E. Scuseria, M. A. Robb, J. R. Cheeseman, G. Scalmani, V. Barone, B. Mennucci, G. A. Petersson, H. Nakatsuji, M. Caricato, X. Li, H. P. Hratchian, A. F. Izmaylov, J. Bloino, G. Zheng, J. L. Sonnenberg, M. Hada, M. Ehara, K. Toyota, R. Fukuda, J. Hasegawa, M. Ishida, T. Nakajima, Y. Honda, O. Kitao, H. Nakai, T. Vreven, J. A. Montgomery Jr., J. E. Peralta, F. Ogliaro, M. Bearpark, J. J. Heyd, E. Brothers, K. N. Kudin, V. N. Staroverov, R. Kobayashi, J. Normand, K. Raghavachari, A. Rendell, J. C. Burant, S. S. Iyengar, J. Tomasi, M. Cossi, N. Rega, J. M. Millam, M. Klene, J. E. Knox, J. B. Cross, V. Bakken, C. Adamo, J. Jaramillo, R. Gomperts, R. E. Stratmann, O. Yazyev, A. J. Austin, R. Cammi, C. Pomelli, J. W. Ochterski, R. L. Martin, K. Morokuma, V. G. Zakrzewski, G. A. Voth, P. Salvador, J. J. Dannenberg, S. Dapprich, A. D. Daniels, O. Farkas, J. B. Foresman, J. V. Ortiz, J. Cioslowski and D. J. Fox, *GAUSSIAN 09, (Revision A.02)*, Gaussian, Inc., Wallingford, CT, 2009.

17 *CYLview, 1.0b; Legault, C. Y*, Université de Sherbrooke, 2009 (http://www.cylview.org).

18 G. A. Zhurko, ChemCraft Home Page: a set of graphical tools for facilitating working with quantum chemistry computations (http://www.chemcraftprog.com).

19 O. T. Summerscales, F. G. N. Cloke, P. B. Hitchcock, J. C. Green and N. Hazari, *Science*, 2006, **311**, 829–831.

20 *Handbook of Preparative Inorganic Chemistry*, ed. G. Brauer, Academic Press, 2nd edn, 1965, vol. 1, p. 485.

21 Y. Zhao and D. G. Truhlar, *J. Chem. Phys.*, 2006, **125**, 194101–194118.